Proceeding Series of the Brazilian Society of Computational and Applied Mathematics, v. 11, n. 1, 2025.

Trabalho apresentado no XLIII CNMAC, Centro de Convenções do Armação Resort - Porto de Galinhas - PE, 2024

Proceeding Series of the Brazilian Society of Computational and Applied Mathematics

Investigation of the Aerodynamic Benefits of Base Bleed Technology on Artillery Shells

Wallace R. R. da Silva[1], Rodrigo A. R. P. Rodrigues[2], André L. T. Rezende[3], Victor S. Santiago[4]
IME, Rio de Janeiro, RJ

Abstract. This article discusses the use of base bleed technology to enhance the range and accuracy of artillery systems. Base bleed technology involves the use of a combustible substance to provide additional thrust to an artillery shell, which reduces drag and increases velocity. To study the phenomena of base bleed technology, the article employs computational fluid dynamics (CFD) using the Finite Volume Method (FVM). A two-dimensional and axisymmetric mesh is constructed, and the RANS turbulence models named Shear-Stress Transport $\kappa - \omega$ are used to simulate the aerodynamic issues involved. The article presents the results of the simulation, including the drag coefficient, pressure and velocity fields. The verification of the range extension generated by the base bleed technology is done with a proprietary MATLAB® code that implements the modified point-mass trajectory model (MPMTM), regulated by NATO (STANAG 4355), and previously validated with commercial software reference for aerospace industry named PRODAS®.

Keywords. Aerodynamics, Ballistic Trajectory, CFD, Turbulence Modeling.

1 Introduction

This text discusses the challenges of extending the range of projectiles in aerodynamics research. The complexity of the problem is due to the influence of compressibility and high Reynolds number. To understand the forces acting on ammunition, various techniques are employed. However, firing tests and wind-tunnel tests can be expensive and difficult to reproduce. Therefore, computational fluid dynamics (CFD) is a cheaper and effective method for studying the aerodynamics of projectiles. The article focuses on the drag force, which is the main contributor to air resistance during flight [3]. There are two principal ways to produce drag: viscous (skin friction drag) and pressure (surface and base drag) [8]. Base drag accounts for approximately 50% of total drag at supersonic speeds. To reduce base drag, a technology called "base bleed" (BB) is commonly used, which involves injecting hot gas to increase base pressure at an optimal value. Ammunition that uses this method is referred to as "extended range" munition (ER).

2 Mathematical Modeling

2.1 Governing Equations

The mass (1), momentum (2) and energy (3) conservation equations for a steady compressible Newtonian fluid flow are represented by [10]:

[1]wrosendoeng@ime.eb.br
[2]rodrigo.azevedo@ime.eb.br
[3]arezende@ime.eb.br
[4]santoro@ime.eb.br

$$\frac{\partial}{\partial x_i}\left(\rho u_i\right) = 0 \tag{1}$$

$$\frac{\partial}{\partial x_j}\left(\rho u_j u_i\right) = -\frac{\partial p}{\partial x_i} + \frac{\partial}{\partial x_j}\left[\mu\left(\frac{\partial u_i}{\partial x_j} + \frac{\partial u_j}{\partial x_i}\right)\right] - \frac{2}{3}\frac{\partial}{\partial x_i}\left(\mu\frac{\partial u_k}{\partial x_k}\right) \tag{2}$$

$$\frac{\partial}{\partial x_j}\left[\rho u_j\left(c_p T + \frac{1}{2}u_i u_i\right)\right] = \frac{\partial}{\partial x_j}\left[\mu u_i\left(\frac{\partial u_i}{\partial x_j} + \frac{\partial u_j}{\partial x_i}\right)\right] - \frac{2}{3}\frac{\partial u_i}{\partial x_i}\left(\mu\frac{\partial u_k}{\partial x_k}\right) + \frac{\partial}{\partial x_j}\left(k\frac{\partial T}{\partial x_j}\right) \tag{3}$$

where u_i, p, μ and T is the velocity, pressure, dynamic viscosity and temperature of the fluid. If the fluid is an ideal gas, therefore ($\rho = p/RT$), which R is the specific gas constant.

2.2 Turbulence Modeling

The SST $\kappa - \omega$ model [6] is a two-equation model that solves for the turbulent kinetic energy κ and the specific dissipation rate ω. This model is a combination of two popular models, the $\kappa - \omega$ model and the $\kappa - \varepsilon$ model, and is designed to provide accurate predictions for a wide range of flows, from low-speed, high-Reynolds number flows to high-speed, low-Reynolds number flows. The SST $\kappa - \omega$ model is particularly effective in predicting flow separation and reattachment, making it a popular choice in aerospace and automotive engineering applications.

2.3 Modified Point-Mass Trajectory Model

The modified point-mass trajectory model (MPMTM) is a resource available to member countries of the North Atlantic Treaty Organization (NATO) [9] through the Standardization Agreement (STANAG) 4355 to provide a standard for the development of firing tables for the analyzed projectiles [5]. The system of equations is as follows [2]

$$\boldsymbol{x}_0 = \begin{bmatrix} 0 & 0 & 0 \end{bmatrix} \tag{4}$$

$$\begin{aligned} m \cdot \dot{\boldsymbol{u}} = &-\frac{\rho v^2}{2} S\left(C_{D_0} + C_{D_{\alpha^2}}\right)\frac{\boldsymbol{v}}{v} + \frac{\rho v^2}{2} S\left(C_{L_\alpha} + C_{L_{\alpha^3}} \cdot \alpha_e^2\right)\boldsymbol{\alpha_e} \\ &- \frac{\rho v^2}{2} S\frac{\varrho d}{v} C_{mag-f}\boldsymbol{\alpha_e} \times \frac{\boldsymbol{v}}{v} + \frac{\rho v^2}{2} S C_{D_{BB}} f(I)\left(\frac{\boldsymbol{v}\cos\left(\alpha_e\right)}{v} + \boldsymbol{\alpha_e}\right) + m\boldsymbol{g} + m\boldsymbol{\lambda} \end{aligned} \tag{5}$$

$$f(I) = \begin{cases} \frac{I}{I_0}, & I < I_0 \\ 1, & \text{otherwise} \end{cases} \tag{6}$$

$$I_x \cdot \dot{\varrho} = \frac{\rho v^2}{2} S d C_{spin}\frac{\varrho d}{v} \qquad \varrho = \varrho_0 + \int_0^t \dot{\varrho} dt \qquad \varrho_0 = \frac{2\pi u_0}{t_c d} \tag{7}$$

$$\frac{\rho v^2}{2} S d\left(C_{m\alpha} + C_{m\alpha^3} \cdot \alpha_e^2\right)\boldsymbol{\alpha_e} = -I_x \varrho \frac{\boldsymbol{v} \times \dot{\boldsymbol{u}}}{v^2} \qquad \boldsymbol{\alpha}_{e_0} = \begin{bmatrix} 0 & 0 & 0 \end{bmatrix} \tag{8}$$

where the position, velocity, and acceleration vectors with respect to the ground are denoted by $\boldsymbol{x}$, $\boldsymbol{u}$ and $\dot{\boldsymbol{u}}$, respectively. Equation (4) indicates the initial firing position. The surface reference area S is calculated using the projectile reference diameter ($\pi d^2/4$). The equation (5) accounts for various forces, including drag (C_{D_0} and $C_{D_{\alpha^2}}$), lift (C_{L_α} and $C_{L_{\alpha^3}}$), Magnus (C_{mag-f}), Base Bleed effect ($C_{D_{BB}}$), gravitational, and Coriolis effects, with corresponding coefficients. The $f(I)$ term represents a function of injection parameter I, whose objective is to relate this parameter to the optimal injection value I_0 (6). The spinning motion of is characterized by the angular velocity ϱ, which depends on the spin damping coefficient C_{spin}, muzzle velocity u_0 and twist rate t_c (7). The model employs an implicit method to calculate the yaw of repose α_e, as described in equation (8).

DOI: 10.5540/03.2025.011.01.0416

3 Description of Proposed Study

3.1 Computational Grid

To formulate the numerical approach required by the finite volume method to be employed in the present work, it was necessary to construct a computational domain through a mesh. With the evolution of the project, an axisymmetric "C"-shaped domain with measurements is created as in Figure 1 (1 with 186,500 elements and other with 380,000 elements), likewise in previous works [4, 7]. The diameter of the outlet nozzle of the Base Bleed system is 2 inches (50.8 mm).

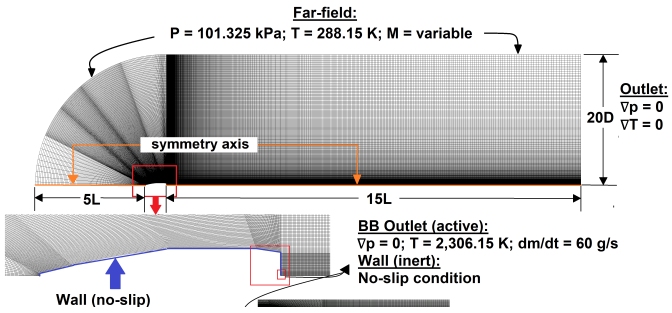

Figure 1: Computational grid. Source: author.

3.2 Necessary inputs

3.2.1 Boundary Conditions

The "Far-Field" region is a region free from the projectile's flow, where air is considered as an ideal gas. The pressure and temperature in this region are determined based on ambient conditions at sea level, and the velocity is determined based on the Mach number. The "Base Bleed Outlet" region represents the flow of gases injected into the projectile's base. The mass flow rate and temperature of these gases are prescribed to determine the velocity, and the pressure at the outlet of the base bleed gases is set to be equal to that of the "Far-Field" region. The "Outlet" region only has prescribed pressure and temperature values. Finally, the "Wall" region is considered adiabatic and has a no-slip condition.

3.3 Modified Point-Mass Trajectory Model Implementation

The modified point-mass trajectory model needs to divide the relevant input data, which was summarized into the Table 1, except for the aerodynamic coefficient data. The process of calculating the aerodynamic coefficients has been made with the PRODAS® software, considering rotational transformations there are differences between STANAG 4355 and PRODAS®, then (9) and (10):

$$C_{D_0} = C_{X_0} \qquad C_{D_{\alpha^2}} = C_{X_{\alpha^2}} + C_{Z_\alpha} - \frac{1}{2}C_{X_0} \qquad C_{L_\alpha} = C_{Z_\alpha} - C_{X_0} \tag{9}$$

$$C_{mag-f} = \frac{1}{2}C_{y_{pa}} \qquad C_{spin} = \frac{1}{2}C_{l_p} \tag{10}$$

Table 1: Inputs for (a) Geometric, (b) Ballistic and (c) Environmental Conditions of MPMTM model

Variable	Value
d	0.1547 m
d_b	0.13373 m
m_{proj}	42.985 kg
m_{prop}	0.5600 kg
I_{x_0}	0.14245 kg/m^2
I_{x_1}	0.13730 kg/m^2
X_{CG_0}	0.45835 m
X_{CG_1}	0.44645 m

(a) Geometric inputs

Variable	Value
I_0	0.005
u_0	878 m/s
θ	711 and 800 mil
latitude	-23π/180 rad
azimuth	0
t_c	25 cal/rev
Q_d	1.2
Q_m	1.2

(b) Ballistic inputs

Variable	Value
$T_{(y=0m)}$	288.15 K
β	6.5 x 10^{-3} K/m
$p_{(y=0m)}$	1.0 atm
$\rho_{(y=0m)}$	1.225 kg/m^3
$\gamma = c_p/c_v$	1.4
$g_{(y=0m)}$	9.81 m/s^2
r_{earth}	6.371 x 10^6 m
ω_{earth}	7.292 x 10^{-5} rad/s

(c) Environmental inputs

4 Results

The software ANSYS 2021R2 [1] was used for geometry construction, meshing, numerical methods, governing equations support, and post-processing of CFD results. The code that implements the modified point-mass trajectory model (MPMTM) has been developed using MATLAB®.

4.1 Drag Coefficient

The drag coefficient values for an artillery projectile with and without the use of Base Bleed were obtained using the SST $\kappa - \omega$ model, as seen in Figure 2. The drag curves of Figure 2a were developed based on the meshes previously mentioned and were compared with the results of Mahmoud et al. [4]. This validation permitted the CFD simulations for different configurations of projectiles (with and without Base Bleed), as seen in Figure 2b.

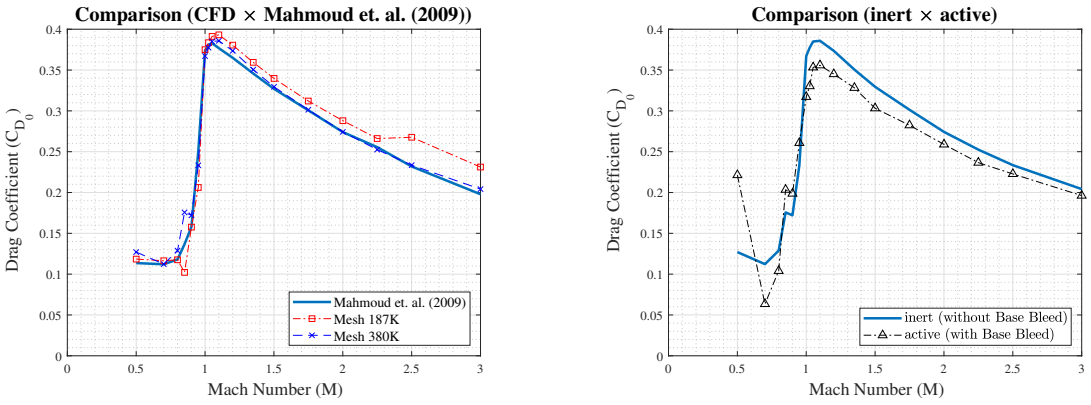

(a) Without Base Bleed

(b) With Base Bleed

Figure 2: Drag coefficient (C_D) of active (with BB) and inert (without BB) projectiles. Source: author.

Comprehending the phenomena caused by Base Bleed technology demands an analysis of pressure and velocity field, especially in the base. Figure 3 shows up the contours of pressure and velocity at Mach 2.0 in the sea level. In the rear region of the projectile, it is noticed that there

are a greater pressure gradient in Figure 3a than in Figure 3b, which means that the Base Bleed system has increased the base pressure.

The velocity contours of Figures 3c and 3d shows the shock wave caused by the supersonic regime and the creation of a low velocity region in the downstream. The Figures 3e and 3f demonstrate what happen with projectile rear region, and the increment of pressure due to Base Bleed system generated a second recirculation zone, which is expected [8]. The consequence in the results is a greater reduction in drag coefficients during the supersonic regime.

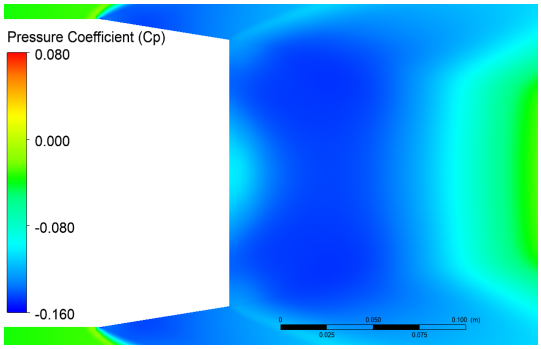

(a) Pressure contours (without Base Bleed)

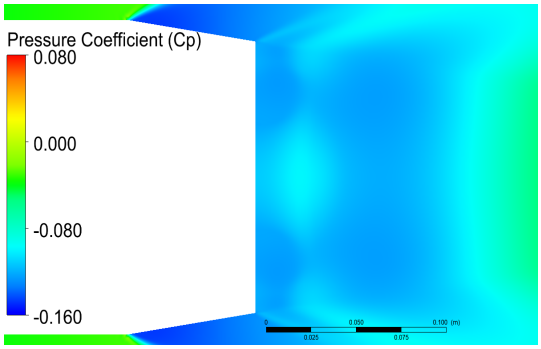

(b) Pressure contours (with Base Bleed)

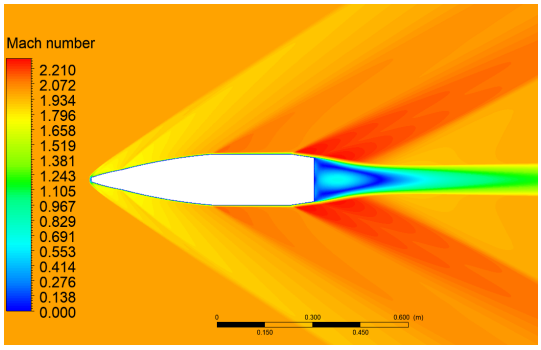

(c) Velocity contours (without Base Bleed)

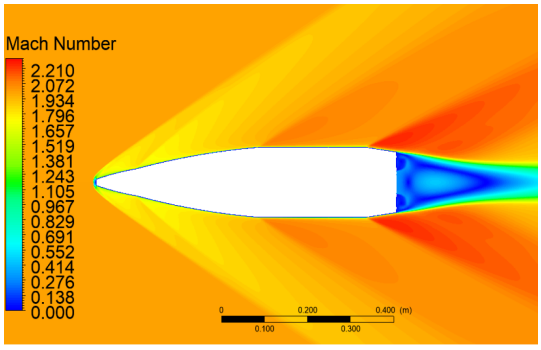

(d) Velocity contours (with Base Bleed)

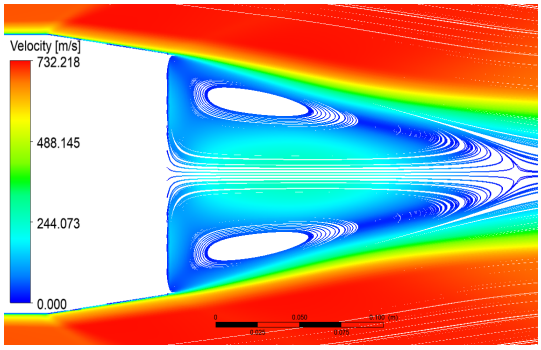

(e) Velocity current lines (without Base Bleed)

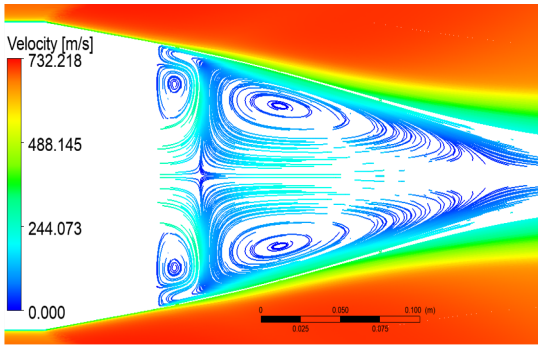

(f) Velocity current lines (with Base Bleed)

Figure 3: Comparison of active (with BB) and inert (without BB) projectiles. Source: author.

DOI: 10.5540/03.2025.011.01.0416

4.2 Comparison of Trajectory with and without Base Bleed

The methodology to prove the Base Bleed efficiency was using the MPMTM trajectory model to calculate numerically the height and downrange of ammunition. The Figure 4 delights the results of flight predictions at muzzle velocity of 878 m/s (Mach 2.58 at sea level) and quadrant elevations (θ) of 711 and 800 mil. The maximum values of downrange and apogee are exposed in the Table 2.

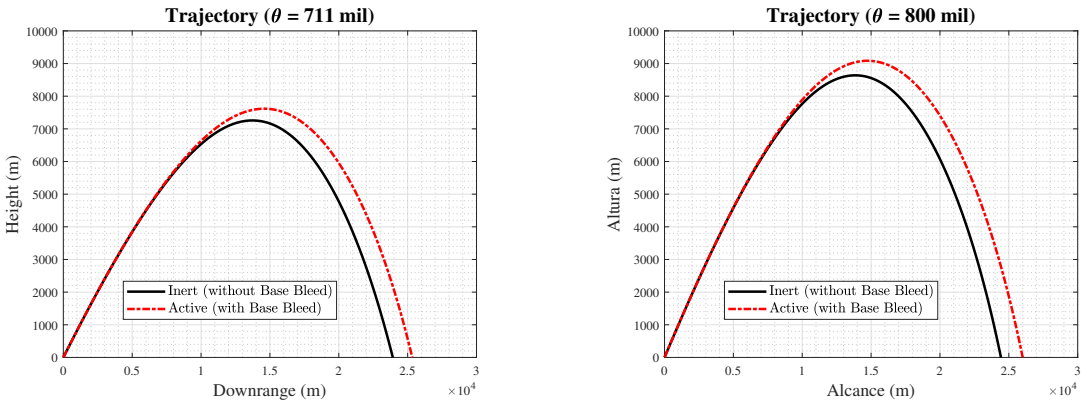

(a) Quadrant Elevation = 711 mil

(b) Quadrant Elevation = 800 mil

Figure 4: Trajectories of active (with BB) and inert (without BB) projectiles for 2 quadrant elevations (θ = 711 mil and 800 mil). Source: author.

When verifying the active projectile with d_{bb} = 50.8 mm, it is noticeable in Table 2 an increment of almost 6.0% in downrange and 5.0% in apogee, even with mass increase at the beginning of firing test at θ = 711 mil. Upon changing the quadrant elevation to 800 mil there is an increase of 6.5% in downrange and a slightly more than 5.0% increase in apogee, which means the the results followed the same of growth order.

Table 2: Ballistic Trajectory at u_0 = 878 m/s with active projectile using mass flow rate ($\underline{m}_{bb}$) = 60 g/s

BB diameter (d_{bb})	Quadrant Elevation (θ)	Downrange	Increment	Apogee	Increment
0 mm (inert)	711 mil	23,922.2 m	–	7,256.8 m	–
0 mm (inert)	800 mil	24,429.5 m	–	8,638.6 m	–
50.8 mm (active)	711 mil	25,334.3 m	5.9%	7,616.6 m	5.0%
50.8 mm (active)	800 mil	26,008.5 m	6.5%	9,084.5 m	5.2%

5 Final Considerations

The study found that implementing Base Bleed technology can affect sensitive parameters, including the ammunition's design, and showed a positive trend in drag coefficient values. However, modeling the interaction between the Base Bleed flame front and turbulent wake proved difficult, and the most relevant parameter affecting drag was the nozzle exit diameter. The program for calculating trajectory was implemented without considering ignition effects or varying propellant burn rate. The study also notes that the simplified projectile geometry used for C_D estimation does not account for the cavity in the base and added propulsion components.

Acknowledgement

We would like to acknowledge the financial support provided by the Coordination for the Improvement of Higher Education Personnel (CAPES) and the National Council for Scientific and Technological Development (CNPq) for this research. We also express our gratitude to the Brazilian Army's Military Institute of Engineering (IME) for providing resources and infrastructure that made this work possible.

References

[1] **Ansys® Academic Research Fluent, Help System, Fluent Theory Guide**. Release 2021R2. USA: Ansys Inc., 2021, p. 1024.

[2] L. Baranowski, P. Majewski, and J. Szymonik. "Explicit form of the "modified point mass trajectory model" for the use in Fire Control Systems". In: **Bulletin of the Polish Academy of Sciences: Technical Sciences** 68.No. 5 (i.a. Special Section on Modern control of drives and power converters) (2020), pp. 1167–1175. URL: http://journals.pan.pl/Content/117694/PDF/22_D1167-1175_01415_Bpast.No.68-5_30.10.20_.pdf.

[3] R. M. Lucena et al. "Numerical Aerodynamic Simulation of an Artillery Projectile with a Base Bleed System". In: **Brazilian Congress of Thermal Sciences and Engineering**. 04 set. 2022. Bento Gonçalves, RS, Brasil: ABCM, 2020, p. 7. DOI: 10.26678/ABCM.ENCIT2020.CIT20-0617. URL: https://abcm.org.br/proceedings/view/CIT20/0617.

[4] O. M. K. M. Mahmoud et al. "Computational investigation of base drag reduction for a projectile at different flight regimes". In: **International Conference on Aerospace Sciences & Aviation Technology**. 25 jun. de 2021. Cairo, Egito: Military Technical College, 2009, p. 14. URL: https://asat.journals.ekb.eg/article_22270_3367f3fe4aaf5352%20ba793eb772bcda01.pdf.

[5] R. McCoy. **Modern Exterior Ballistics: The Launch and Flight Dynamics of Symmetric Projectiles**. 2nd ed. Atglen, USA: Schiffer Publishing, 2012, p. 328.

[6] F. R. Menter. "Review of the shear-stress transport turbulence model experience from an industrial perspective". In: **International Journal of Computational Fluid Dynamics** 23.4 (2009), pp. 305–316. DOI: http://dx.doi.org/10.1080/10618560902773387.

[7] F. Nicolás-Pérez et al. "On the accuracy of RANS, DES and LES turbulence models for predicting drag reduction with Base Bleed technology". In: **Aerospace Science and Technology** 67 (2017), pp. 126–140. ISSN: 1270-9638. DOI: https://doi.org/10.1016/j.ast.2017.03.031. URL: https://www.sciencedirect.com/science/article/pii/S1270963816302577.

[8] J. Sahu and K. R. Heavey. "Numerical Investigation of Supersonic Base Flow with Base Bleed". In: **AIAA Journal** 34.1 (1997), pp. 62–69. URL: https://doi.org/10.2514/2.3173.

[9] **The Lieske Modified Point Mass and Five Degrees of Freedom Trajectory Models - AOP-4355 EDITION A**. 3rd ed. Organização do Tratado do Atlântico Norte. Washington DC, Estados Unidos da América, 2009, p. 95.

[10] D. C. Wilcox. **Turbulence Modeling for CFD**. 3rd ed. La Cañada: DCW Industries, 2006, p. 522.

